#### **RESEARCH**



# Genetic heterogeneity in p53-null leukemia increases transiently with spindle assembly checkpoint inhibition and is not rescued by p53

Mai Wang<sup>1</sup> • Steven Phan<sup>1</sup> • Brandon H. Hayes<sup>1</sup> • Dennis E. Discher<sup>1</sup>

Received: 3 February 2023 / Revised: 8 May 2023 / Accepted: 16 May 2023 / Published online: 31 May 2023 © The Author(s), under exclusive licence to Springer-Verlag GmbH Germany, part of Springer Nature 2023

#### Abstract

Chromosome gains or losses often lead to copy number variations (CNV) and loss of heterozygosity (LOH). Both quantities are low in hematologic "liquid" cancers versus solid tumors in data of The Cancer Genome Atlas (TCGA) that also shows the fraction of a genome affected by LOH is ~ one-half of that with CNV. Suspension cultures of p53-null THP-1 leukemia-derived cells conform to these trends, despite novel evidence here of genetic heterogeneity and transiently elevated CNV after perturbation. Single-cell DNAseq indeed reveals at least 8 distinct THP-1 aneuploid clones with further intra-clonal variation, suggesting ongoing genetic evolution. Importantly, acute inhibition of the mitotic spindle assembly checkpoint (SAC) produces CNV levels that are typical of high-CNV solid tumors, with subsequent cell death and down-selection to novel CNV. Pan-cancer analyses show p53 inactivation associates with aneuploidy, but leukemias exhibit a weaker trend even though p53 inactivation correlates with poor survival. Overexpression of p53 in THP-1 does not rescue established aneuploidy or LOH but slightly increases cell death under oxidative or confinement stress, and triggers p21, a key p53 target, but without affecting net growth. Our results suggest that factors other than p53 exert stronger pressures against aneuploidy in liquid cancers, and identifying such CNV suppressors could be useful across liquid and solid tumor types.

 $\textbf{Keywords} \ \ \text{Aneuploidy} \cdot p53 \cdot Spindle \ assembly \ check \ point \ (SAC) \cdot Liquid \ tumor \cdot Hematologic \ cancer$ 

#### Introduction

Aneuploidy can have important roles in human cancer initiation and progression. For example, Down syndrome (trisomy-21) shows leukemia rates that are 150-fold higher than normal (Wagenblast et al. 2021). A pan-cancer analysis further shows a particularly high correlation between loss of a chromosome and scored loss of a tumor suppressor gene for that chromosome—with frequent loss of chromosome-17 likely explained by its harboring of *TP53* (Davoli et al. 2013). For some cancers, aneuploidy is prognostic of poor survival (Ponnapalli et al. 2020; van Dijk et al. 2021) and favors drug resistance (Lukow et al. 2021). Aneuploidy has long been noted in ~90% of solid tumors but only ~50% or fewer hematologic or "liquid" cancers (Beroukhim et al. 2010; Xian et al. 2021), and a deeper understanding of any limits to liquid cancer aneuploidy might be generally useful in broadly suppressing aneuploidy in many types of cancer.

We focus on liquid suspension cultures of THP-1, an acute monocytic leukemia cell line that is deficient in TP53, and our findings are put in a broader pan-cancer context. To assess heterogeneity of CNVs and aneuploidy that ranges from whole chromosome to focal or segmental, we applied single-cell sequencing methods to THP-1's as well as bulk analyses after single cell expansion (Table 1). We exploited an MPS1 kinase inhibitor that increases mitotic mis-segregation (Stucke et al. 2002) in order to assess genetic heterogeneity shortly after drug treatment and much later. Transient diversification proves similar to or greater than a majority of solid tumors, and subsequent down-selection creates new genetics that again argues against a unique aneuploid state for this suspension cancer line. By further assessing the genetic changes before and after introducing TP53 back to the cell line, we conclude that this key genome stability factor (Toufektchan & Toledo 2018) is more important upstream than downstream in suppressing aneuploidy. The observation aligns with recent findings (Baslan et al. 2022), but we find that p53 can affect survival under some chemical and physical stressors relevant to the microenvironment.



Dennis E. Discher discher@seas.upenn.edu

Molecular & Cell Biophysics Lab, University of Pennsylvania, Philadelphia, PA 19104, USA

**Table 1** Summary of an euploidy type that is reported based on different technologies or data sources

Technology/data source	Aneuploidy reported
TCGA/CCLE	Focal/segmental changes
Single-cell DNAseq	Arm-level changes
Single-cell RNAseq	Whole chromosome changes
Single nucleotide polymorphisms	Focal/segmental changes

#### Results

# CNV and LOH are proportional but low for liquid cancers, including THP-1 line lacking TP53

Measurements of CNV versus LOH are respectively based on amounts of sequence versus specific sequence of alleles, and different methods have different sensitivities for the two types of measurements. LOH can be complex such as a loss followed by duplication of the allele, which yields copy-neutral LOH. Recent pan-cancer analyses of The Cancer Genome Atlas (TCGA) nonetheless suggest a correlation between the median proportion of LOH and median number of CNV segments, even though most cancers (21 of 33) lie outside of the 95% confidence interval (including the two liquid cancers in TCGA) (Steele et al. 2022). We take a slightly different approach and find a far more significant proportionality (Fig. 1a: p < 2.2e-16;  $R^2 = 0.94$ ) between the average fraction of chromosomes with LOH versus the average fraction of chromosomes with CNV based on recently curated TCGA results (Knijnenburg et al. 2018). A fitted slope of 0.41 is close to a theoretical ½ for a simple model wherein half of any CNV is a loss that yields an LOH. Moreover, a shallower slope suggests a greater frequency and tolerance for aneuploidy relative to LOH. Fitting well to these trends is the averaged patient data for the liquid cancer with the least genome variation, LAML (acute myeloid leukemia), and also our own bulk genetics results for an LAML-derived, suspension culture line THP-1 that is of primary interest here.

To further relate key pan-cancer trends to such metrics of genetic change, we compared the quartile of patients with the most CNV to those with the least. Poor survival for high CNV is clear and significant in only 7 of 33 cancer types (p < 0.05), and nearly all are low in CNV and LOH, including LAML (Fig. 1a-bottom, Fig. S1). High aneuploidy cancer types (e.g., SKCM, skin cancer melanoma) might be so variable and heterogeneous that there is little difference between patients with average high and low aneuploidy. The survival trend is distinct from cell cycle and is highest for high CNV patients in about half of

all cancer types across the aneuploidy scale. This is based on a multi-gene cell cycle score (CCS) as well as standard cell cycle markers MKI67 and TOP2A (Fig. 1a-bottom). Interestingly, for low aneuploidy cancers such as LAML, high CNV and high LOH do not associate with cell cycle but both do associate with TP53 inactivation (Fig. 1a-bottom, SI. 1a). This analysis was done with a machine-learning-based TP53 classifier (Knijnenburg et al. 2018) and RNA-seq expression of TP53-interacting genes, yielding an inactivation score of 0 to 1. The pan-cancer analysis of high CNV patients shows a peak for cancer types with mid-level aneuploidy (Fig. 1a-bottom). Overall, these various analyses of TCGA have multiple implications, but LAML is particularly interesting as one of only three cancer types for which high CNV patients show both poor survival and high inactivation of p53.

Aneuploidy analyses of the Cancer Cell Line Encyclopedia (CCLE) likewise indicate that leukemia lines possess relatively low CNV levels (Fig. 1b). Lymphoma lines tend to have higher CNV, consistent with TCGA analyses of DLBC (diffuse large B-cell lymphoma) relative to LAML as the only two liquid cancers, and solid tumor-derived lines tend to have even higher CNV levels, consistent again with TCGA (Fig. 1a). Interestingly, recent studies suggest DLBC progresses as a more solid-like tumor mass (Shah et al. 2023), which might explain the trend DLBC > LAML. THP-1 cultures nonetheless fit within the trends and are reported from bulk methods to be modestly an uploid and have moderate LOH, including one copy of TP53 that is truncated. Such results are confirmed by our THP-1 analyses with bulk single nucleotide polymorphism array (SNPa) and with singlecell RNA-seq that showed very few TP53 transcripts relative to normal monocytes (Fig. 1c). Our results also agree with bulk measurements obtained over several decades (Sugimoto et al. 1992). The THP-1 cell line thus seemed a reasonable candidate LAML cell line to better characterize genome heterogeneity, perturbations, and growth/death, as well as some effects of rescue by p53 overexpression.

# Heterogeneity of THP-1 genetics increases with MPS1i, while doubling time scales with LOH

Genetic heterogeneity of THP-1 liquid cultures has not been described previously. *TP53* inactivation suggested that some heterogeneity are likely. We used single-cell DNA-seq to identify CNV and high-dimensional uniform manifold approximation and projection (UMAP) to illustrate relationships between 8 distinct subclones (Fig. 1d). CNV profile of primary clone C1 requires only one arm-level copy number alteration to transform into one of the other subclones as denoted by the labeled UMAP plot. For comparison, 6 subclones were identified for the B16F10 murine melanoma



cell line (SI. 3a), which is known to maintain functional p53 but also to be highly aneuploid (Zhou et al. 2020) consistent with human melanoma (SKCM in Fig. 1a). The nominal consensus sequence (73% of cells) shows arm-level CNV largely limited to chromosome 12p (Fig. 1d). Nonetheless, some of the major clones including C1 also have abnormal cells with clear losses or gains of whole chromosomes (Fig. 1d table). This further emphasizes THP-1 heterogeneity and suggests ongoing genome instability in this suspension-grown line.

To test the possible effects of genetic perturbation and diversification of THP-1's and also assess the overall evolution toward old or new CNV states, we used an MPS1 kinase inhibitor reversine that is known to increase CNV in solid tumor-derived lines. Its effects on suspension cultures are under-studied (Bolton et al. 2016; Santaguida et al. 2017), especially any transient or sustained genetic evolution, and so we performed single-cell expansion of THP-1 suspension cultures over 2 months (Fig. 2a). MPS1 is an essential regulator of the SAC that maintains genomic stability by delaying division until all chromosomes properly orient (Liu & Winey 2012). SNPa measurements of CNV and LOH for bulk and for each clone show agreement of bulk with single-cell DNAseq consensus (Fig. 2b), and also show that all five of the untreated clones analyzed share a CNV signature with one of the 8 main subclones found in the single-cell DNA-seq analysis, which confirms the THP-1's heterogeneity (Fig. 2b). Furthermore, THP-1's treated with reversine followed by clonal expansion yield 2-of-5 clones (40%) with unique CNV that are absent from the untreated population (Fig. 2b table).

For each single-cell clone, the fraction of the genome with CNV or LOH was compared to the LAML patients in the TCGA database, and we also included an indication of *TP53* expression levels as high, medium, or low (Fig. 2c). Interestingly, the linear fit of LAML patients is nearly the same as that of the earlier pan-cancer fit (Fig. 1a). For THP-1's regardless of reversine treatment or not, the cells show a higher aneuploidy and LOH level compared to nearly all LAML patient samples except for those with the lowest *TP53* expression levels. Such a result is consistent with *TP53* inactivation in THP-1 cells (Fig. 1c), and suggests that such liquid cancers are limited to aneuploidy and LOH states that are typical of only about one-third of solid tumors (i.e., those that are less aneuploid in Fig. 1a vs Fig. 2c).

Doubling times of various clones that were reversine-treated or not show a strong correlation with LOH levels (Fig. 2d) (but not CNV fraction, SI. 4e), and reversine-treated clones also showed 2–threefold larger variations in both doubling times and LOH. LAML patients with high LOH in TCGA (<25 patients) showed no significant bias toward high or low cell cycle relative to the other LAML patients (Fig. S1), but the cohort might be too small given the noted variation. In bulk cultures with two different

reversine protocols, overall proliferation is impeded in the first few days and cell death increases ~2—threefold or more beyond ~4 days (Fig. 3a, b). More cells also accumulate in late cell cycle with reversine, suggesting a G2/M arrest, and some show high DNA content suggesting polyploidy (Fig. 3c). Such results suggest a diversification of the genetics by MPS1 inhibition, leading to a selection via lack of viability for some genotypes and slower growth for others.

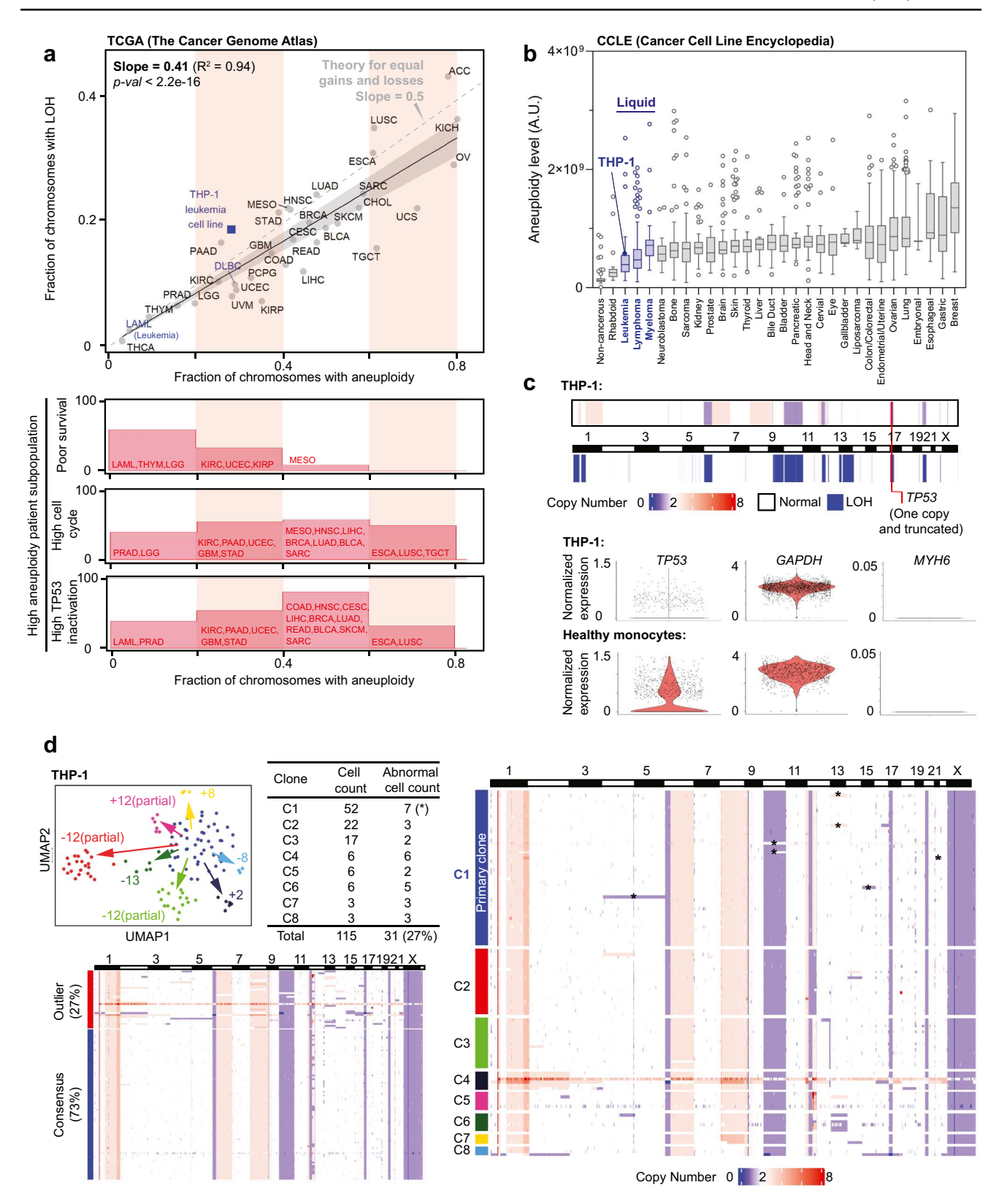
To assess such variation and gain insight into THP-1 phenotype, we used single-cell RNA-seq after reversine treatment and either a 2-day or a 2-week recovery period. We inferred copy number from single-cell RNA-seq data and used healthy monocytes as a reference (see inferCNV in methods, SI. 5). For the untreated and DMSO controls, the inferred CNV and heterogeneity measures of 21-25% outliers with whole Chr gains or losses (Fig. 3d) align well with the CNV profiles from DNA-seq and the 27% outliers (Fig. 1d). A deviation measure for the outlier cells is also highly relative to the CNV of the consensus population. Two days after the reversine treatment (a couple of normal cell cycles), the outlier cells remain similar in relative amount (19 vs 21%), but the ~ twofold higher deviation of the outliers is much greater than control outliers and with more frequent diversification or "entropy" in copy number gains and losses (Fig. 3e). The results indicate an abrupt and drastic change of genotype within the affected THP-1 cells. Importantly, the results suggest the fraction of chromosomes with an euploidy increases from ~0.3 for control THP-1 up to nearly  $\sim 0.6$  for the outlier cells, which is typical of high-CNV solid tumors such as lung cancer and melanoma (LUAD, SKCM in Fig. 1a, SI. 6a).

The RNA-seq data was further used to assess the cell cycle score (CCS) for the treated and untreated outliers relative to the consensus cells, and the results indicate no perturbation or correlation to cell cycle in the high deviation cells (Fig. 3e). LAML patients also showed no overall correlation between high aneuploidy and cell cycle, unlike some other cancers (Fig. 1a).

After a 2-week recovery from reversine, inference of CNV from single-cell RNA-seq shows that the outlier population is ~ twofold higher (42 vs 21%, Fig. 3d). However, the deviation and entropy both recover to low control levels. Unique chromosome gains and losses are nonetheless observed in multiple cells, such as Chr 3 loss (not found in either DNA-seq or RNA-seq of the controls). This further supports the induction and tolerance in the suspension culture viability of new THP-1 genotypes.

The findings argue against a unique aneuploid state for this suspension cancer line and seem consistent with the heterogeneity of unperturbed cells (Fig. 1d). Artificially induced genetic alterations can be expected to render survival and growth differences. Indeed, at least one of the unique clones studied 2 months after reversine treatment







**∢Fig. 1** Loss of heterozygosity (LOH) is proportional to aneuploid (CNV) fraction of chromosomes, with both being low in hematologic liquid cancers, and (unlike many cancers) leukemia patients with high aneuploidy show poor survival and also inactivated TP53 similar to the THP-1 leukemia line. Table 1 reports the aneuploidy measure for each method used. a TCGA data demonstrates linearity between the fraction of chromosomes with LOH and the fraction of chromosomes with CNV in various cancer types (error bands indicate 95% confidence interval, slope=0.41,  $R^2$ =0.94, p-val<2.2e-16). Liquid tumor patients (LAML and DLBC, in blue font) have low levels of both CNV and LOH among all cancers. Data for the THP-1 line is described below. Bar plots at the bottom further indicate the percentage of cancers with poor survival, high cell cycle gene expression, and high TP53 inactivation among patient subpopulations with high aneuploidy (top 25% vs bottom 25% based on fraction of genome with CNV in each type of cancer; cancer types with significant differences were labeled on the bar plot). Cancer type abbreviations are standard per TCGA. b Aneuploidy level of different cancer cell lines from Cancer Cell Line Encyclopedia (CCLE). The plot was summarized based on the disease types and arranged based on the upper quantile aneuploidy level. Leukemia has a similarly low level of aneuploidy when compared to many non-cancerous cell lines. Suspension cancer cell lines (blue) indeed tend to possess very low aneuploidy. c Characterization of TP53 in THP-1. SNPa shows a single copy of TP53 on chromosome 17, but single-cell RNA-seq suggests near zero TP53 transcript in THP-1 cells. Single-cell RNA-seq of healthy monocytes from human peripheral blood mononuclear cells (PBMCs) serves as a control of normal expression level of TP53. GAPDH is a commonly expressed gene and MYH6 served as a null expression control due to its sole expression in cardiomyocytes. d Heterogeneity in UMAP and clustering analysis over copy number results from our single-cell DNA-seq of THP-1 s shows 8 different subclones. Cells in each clone share unique CNV features which differentiate them from the primary clone C1 (denoted in the UMAP plot). Tabulated cell numbers of each clone include those deemed abnormal. Cells with arm-level chromosome changes compared to the primary clone were denoted as "outliers," and outliers of C1 were marked by asterisks

showed the slowest growth (and highest LOH) versus the many other clones studied (in Fig. 2c, d). All of these findings lead us to conclude that the SAC plays an essential role in the genetic integrity of a suspension culture that is p53-null, which prompted us to begin studying p53.

# CNV trends with TP53 inactivation in LAML, but p53 overexpression does not rescue CNV

Inactivation of "guardian of the genome" p53 is perhaps the most common feature across human cancers (Lane et al. 2010). This has motivated development of p53-based therapies, some of which have been approved in a few countries (Wallis et al. 2023), but many issues remain such as coaggregation of mutant p53 with remaining WT p53 (Wallis et al. 2023). In LAML patients, TP53 inactivation tends to increase with CNV and LOH (Fig. 4a, SI. 7a, b) as widely reported (Gonzales & Cheok 2018; Prokocimer et al. 2017). Less appreciated perhaps is that the LAML correlation is far weaker and noisier (slope=0.32;  $R^2$ =0.31) than the pan-cancer correlation across solid tumors (slope=0.80;  $R^2$ =0.80)

(Fig. 4b). For some cancer types, p53 inactivation is considered a frequent first step toward CNV generation (Baslan et al. 2022), but LAML's weaker trend not only suggests a weak regulation by p53 but also again indicates a relative limit to aneuploidy in this liquid cancer. This observation seems consistent with the weak effects of reversine in the long term (Fig. 2a–d).

To test the above hypothesis, we introduced wild-type TP53 into the THP-1. Although correction of such a significant and clinically relevant deletion (Welch 2018) by gene editing might eventually prove efficient, we chose to transduce full length p53 by Lentivirus to assess rescue in THP-1. Western blot confirms protein expression (Fig. 4c), based on an anti-p53 against the so-called TAD1 region, which was chosen because isoforms lacking TAD1 associate with poor prognosis (Avery-Kiejda et al. 2014) compared to other isoforms (Bourdon et al. 2011; Joruiz & Bourdon 2016). We observe that p53 levels in these THP-1 cells are equal to or greater than those in the p53-normal A549 lung adenocarcinoma cell line (SI. 8a). Importantly, copy number profiles of clones show minimal differences between the wild-type and p53 overexpressing THP-1 (TP53OE THP-1) (Fig. 4d). Such a finding aligns with the past conclusions that p53 loss is usually upstream of aneuploidy generation rather than a downstream effector (Baslan et al. 2022).

### TP53 overexpression in THP-1 favors apoptosis ± stress

Apoptosis in response to DNA damage can be induced by p53 for some cell types (Aubrey et al. 2018), but effects in THP-1 cells have remained unclear. TP53OE cells have a doubling time that might be slightly longer than control THP-1 cells, but TP53OE cells certainly have a~twofold higher cell death rate in standard culture (Fig. 4c, e). Oxidative stress is typical in many diseased microenvironments. Treatment of multiple cell types with the oxidative stressor H<sub>2</sub>O<sub>2</sub> triggers apoptosis through a mitochondrial pathway with activation of effector caspase-3 dependent in part on p53 via p38 MAPK (Bejarano et al. 2011; Lee et al. 2012; Li et al. 2010; Roy et al. 2010; Shi et al. 2021; Sies & Jones 2020). Studies of THP-1 in this context are lacking, but we find that H<sub>2</sub>O<sub>2</sub> increases cell death generally and maximally for the TP53OE cells (Fig. 4e). The results are thus consistent with rescue of an anticipated p53 activity. In contrast to  $H_2O_2$ , cell death with the drug PFT- $\mu$  proves independent of p53 (Fig. 4e). This drug induces apoptosis in acute leukemia via HSP70 inhibition (Kaiser et al. 2011) and might also inhibit p53 (Chipuk et al. 2004; Leu et al. 2004; Mihara et al. 2003).

Within the bone marrow microenviroment, proliferation of leukemia cells can exert a confinement pressure against bone that is sufficiently large to expand the marrow and cause bone infarction and pain (Li et al. 2019). We simulated such



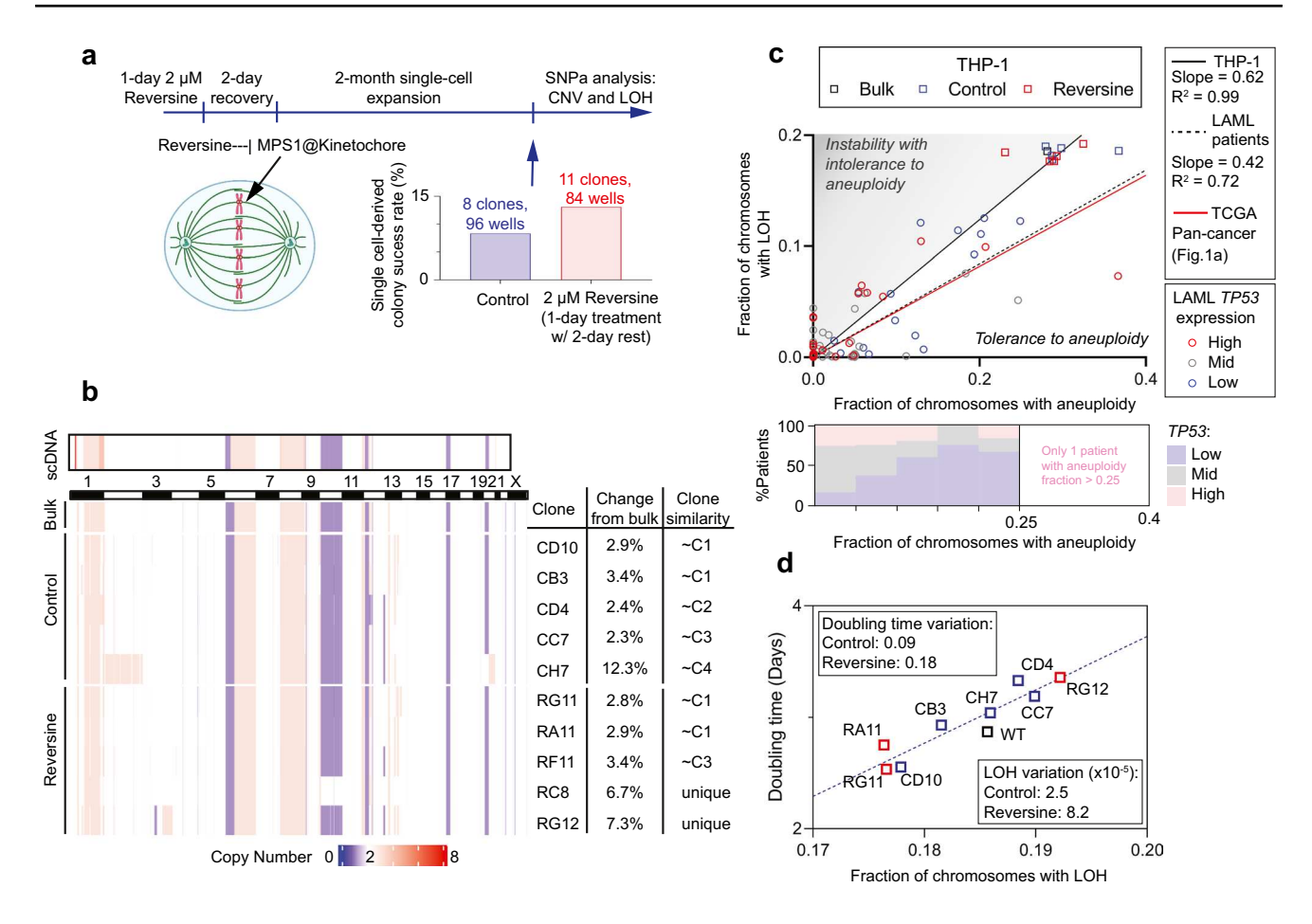


Fig. 2 Single-cell THP-1 expansion reveals tolerance to intrinsic and inducible genomic variation. a Experimental setup of single-cell THP-1 expansion. In short, serial dilution was performed to grow THP-1 developed from a single cell for 2 months. The cells were either untreated or treated by 2 µM reversine, a potent MPS1 kinase inhibitor, followed by a 2-day recovery period before expansion. Bar plot below represents the success chance of a single cell developing into a clone under 2 different conditions. Reversine-treated samples have a slightly higher success rate of expanding into clones. **b** Copy number profile of the single-cell clones derived from SNPa. CNV results from single-cell DNAseq on top perfectly match the SNPa results derived from the general THP-1 population (labeled as "bulk"), confirming the validity of SNPa inferred copy number. Most of the single-cell clones developed can be traced back to the subclones derived from Fig. 2a based on the shared copy number profiles. However, some reversine-treated clones acquired CNV signatures there were missing from the DNAseq data (labeled as

"unique"), highlighting the potential generation of viable clones with new chromosome changes through MPS1 kinase inhibition. c LOH level correlates to CNV level within LAML patients, and high CNV/ LOH patients tend to have high TP53 expression. Patients/cells are considered to be TP53 high/low if they are top/bottom 25% in p53 expression. THP-1 (square) that is known to be TP53 deficient has a much higher aneuploidy and LOH level compared to patient samples (circle). The best-fit lines of single-cell clones, TCGA LAML patient data, and TCGA pan-cancer data were drawn on the plot. Different colors were used to indicate the treatment condition of single-cell clones and TP53 expression status in LAML patients. The bar plot below shows that LAML patients with high CNV level tends to be low in TP53 expression in TCGA database. d Proliferation rate of the single-cell clones correlates to their LOH levels. Reversine-treated clones tend to have high variance both genetically and phenotypically. Table 1 reports the aneuploidy measure for each method used

physical stress by 8-h compression of THP-1 cells and again measured death (Fig. 4f). Confinement increases apoptosis in both wild-type and TP53OE cell lines, with slightly more apoptosis induced by p53 than expected for proportional effects beyond untreated controls (dashed line with unit slope in Fig. 4g). With PFT-μ which can inhibit p53, any p53-dependent increase in death for TP53OE is understandably below the same trend line (Fig. 4g). The results suggest the possibility that more sustained physical and chemical stressors

(e.g., months instead of hours and days) could bias the death of specific genotypes and drive p53-dependent selection, but new genotypes might also be induced under stress.

### p53 expression in THP-1 activates p21 in stressed cells

After verifying that the low level of *TP53* expression in THP-1's is unaffected by MPS1i (SI. 9a), we sought to



determine which if any of the canonical p53-activated genes might be affected (SI. 9b). The cyclin-dependent kinase inhibitor-1 p21 is a well-known major target of p53 and is the only gene showing a significant increase with MPS1i treatment—although transcript levels are minimal (SI. 9c).

To assess activation p21 of protein in both wild-type and p53 overexpressing THP-1's, we used Western blotting methods (SI. 10) after treatments with MPS1i or etoposide that induces DNA damage (Walles et al. 1996). Low levels of p21 are detected in wild-type and p53 overexpressing THP-1's, and p21 is unaffected by drug treatments of wild-type THP-1 s (Fig. 5a, b). In comparison, etoposide causes a strong and clear increase only with p53 overexpression (Fig. 5c). As controls, two adherent cancer cell lines that express p53, U2OS, and A549 also show strong increases of p21 protein with etoposide (Buscemi et al. 2014) with less induction by MPS1i.

Upregulation of p21 causes downregulation of many cell cycle genes (Engeland 2022), and the drugs cause a clear suppression of growth immediately after treatment (Fig. 5d)—but the effects are the same for wild-type and TP53OE cells. The lack of obvious p53 effect is surprising given the p21 activation (Fig. 5c). However, the results again suggest key pathways that are p53-independent in THP-1 cells.

#### **Discussion and conclusions**

Biophysical differences between liquid and solid tumors conceivably contribute to differences in genome instability. Liquid tumors flow easily in dispersing throughout the body and are generally said to exhibit far fewer chromosome gains and losses compared to solid tumors that are typically more confined even at metastatic sites. Liquid cancers also show a more balanced rate of chromosome gains and losses (Duijf et al. 2013). Such differences in liquid and solid tumors could reflect fundamentally different etiologies, ranging from induction of diversity to subsequent selection pressures that are intrinsic or extrinsic to such different types of cells.

We focused on the SAC and p53 because CNV is caused by chromosome segregation errors (Cimini et al. 2001). Based largely on studies in adherent cell types from solid tumors and tissues, the SAC's MPS1 kinase blocks anaphase onset and ensures proper mitotic orientation (Dudka et al. 2018), but chromosome mis-segregation can trigger p53-dependent fail-safe mechanism to block proliferation and aneuploidy (Hinchcliffe et al. 2016). Using single-cell sequencing, we traced the changes of CNV heterogeneity in liquid suspension cancer lines with either short-term or long-term MPS1i and concluded that MPS1 kinase in a typical liquid cancer line is functionally important. Diversification can be initially large and similar to levels sustained in solid tumors. Novel CNV can clearly emerge and impart a growth advantage (Ben-David & Amon 2020;

Weaver et al. 2007). Such findings here are consistent with an unappreciated tolerance in liquid cancers to initial genetic heterogeneity, and have implications for resistance to therapy. Nonetheless, long-term tolerance to CNV heterogeneity seems to be at a low basal level. Microenvironment-relevant chemical and physical perturbations applied to liquid suspension cancer cells expressing *TP53* or not show that p53 does not rescue pre-existing copy number defects. Nonetheless, p53 remains functional in favoring slight apoptosis under stressful conditions of likely relevance to CNV.

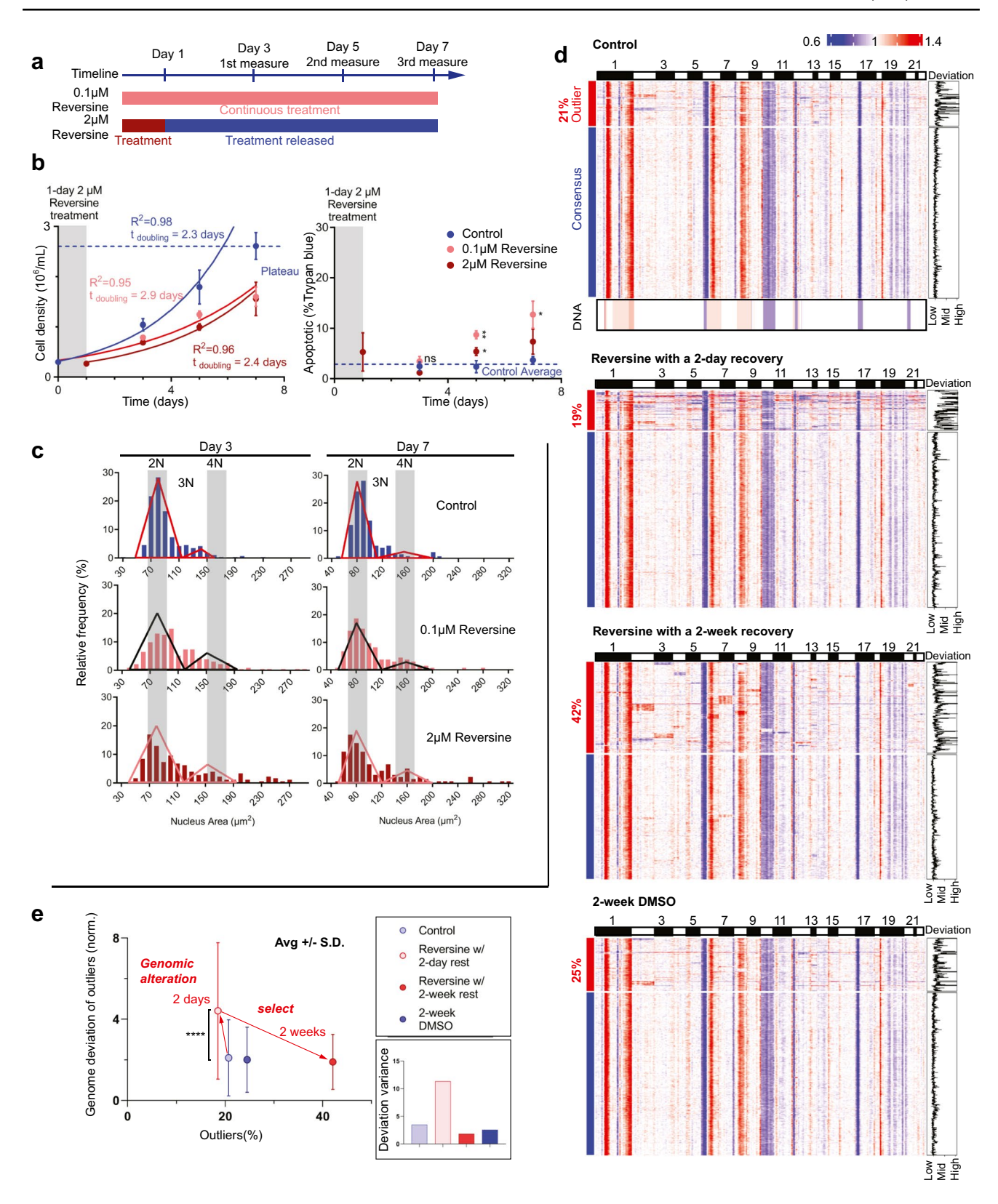
Expression of p53 is reported to relate to pluripotency of human embryonic stem cells (Fu et al. 2020). We therefore assessed pluripotency marker expression among LAML patients with high and low p53 inactivation in TCGA. No significant differences are observed between the groups (SI. 11).

Cancer progression is not only driven by internal genomic factors, but also by microenvironment factors that include biophysical factors such as confinement. Tumor stiffness relates closely to cancer progression and metastasis of solid tumors (Mierke et al. 2018; Wei et al. 2017), and external plus internal factors can contribute to co-evolution (Emon et al. 2018). Physical stress applied to solid cancer derived lines generates DNA damage in part via mis-localization of DNA repair factors (Xia et al. 2018). Liquid cancers are understudied in such contexts despite physical diversity in liquid cancer microenvironments. Mechanotransduction factors are indeed upregulated in malignant non-adherent cancer cells (Wong et al. 2018). Bone marrow is typically pliable but is adjacent to rigid bone and also separated from flowing blood by a restrictive basement membrane (Ivanovska et al. 2017), which suggests sources of physical "stress" and which motivated us to begin studying confinement effects on suspension cultures. Our finding of increased cell death under confinement shows that liquid cancers are sensitive to mechano-environment, which begins to indicate that biophysical cues might play an important role in liquid cancer genetics whether by selection or induction.

We evaluated p21, one of the well-known downstream targets of p53, in order to further assess function of ectopic p53 in the THP-1 suspension cancer line. Our findings clearly indicate that p53 rescues p21 activation in THP-1's with DNA damage caused by Etoposide. However, the expected growth suppression is independent of p21 level. Furthermore, p53 level within the engineered suspension cancer line decreases after receiving reversine and etoposide (Fig. 5c), which is opposite to the trend observed in the two solid tumor-derived adherent cancer cells studied. All of these findings suggest distinct p53 pathways.

Overall, our experimental studies plus analyses of pancancer TCGA data suggest that there are mechanisms beyond p53 for relatively strong genetic protection in liquid cancers compared to solid tumors. Further understanding of such mechanisms may enable new strategies in suppressing genetic diversity that impacts cancer therapy and resistance.







**∢Fig. 3** MPS1 kinase inhibition suppresses suspension cell line proliferation and transiently increases CNV entropy with subsequent selective growth of unique CNV, as inferred from single-cell RNAseq. a THP-1 cells received either continuous low-dose or short-term high-dose reversine treatment for proliferation rate assessment. b MPS1 kinase inhibition suppresses THP-1 growth and lead to a minor increase in cell death percentage after day 4. c Cell cycle analysis over THP-1 s with MPS1 kinase inhibition shows an increase in the percentage of G2/M cells, suggesting G2/M arrest. d Inferred copy number using single-cell RNA-seq shows high resemblance to single-cell DNA-seq results (labeled as "DNA"). Cells labeled as "outlier" have arm-level chromosome gains and losses compared to the consensus copy number profile of the entire population. Deviation measures the difference of inferred CNV level between each cell and the consensus population. The deviation has been normalized such that the averaged deviation of the consensus population equals to 1. Table 1 reports the aneuploidy measure for each method used. e Plot of outliers' deviation against percent of outliers in various conditions. Outliers' deviation score from reversine-treated THP-1 has a drastic increase right after the treatment and decreases to near normal level after a 2-month recovery period. However, the percent of outliers increase after the 2-month recovery. The inset represents the variance of the deviation. Reversine-treated THP-1 with short-term recovery has a very high variance compared to the other samples, suggesting high CNV heterogeneity in the population

#### **Materials and methods**

### TCGA Analysis and cell cycle gene expression score calculation

Expression (RNA-seq, rsem reads), copy number variation (masked cnv), and phenotype data was downloaded from UCSC Xena website (https://xenabrowser.net/datapages/) (Goldman et al. 2020). For scaling analysis, patients of each cancer type were categorized based on the fraction of chromosomes with CNV/LOH. Top 25% of the patients were compared to the bottom 25% over the CCS, survival rates, and *TP53* inactivation score. For CCS and *TP53* inactivation score comparison, Welch's *t*-test was used. For survival rate, Kaplan–Meier curves were generated, and the log rank test was used. The *p*-values were reported (SI. 1a). Cancer types showing significant differences between high vs low CNV/LOH groups are labeled in Fig. 1a.

For CCS calculation, *z*-scores of the rsem reads from cell cycle genes were computed. The cell cycle gene list was obtained from a well-curated aggregation of three different databases (Lundberg et al. 2022). The *z*-scores of all the cell cycle genes were summed in each cell and scaled between 0 and 1 as CCS.

#### **CCLE** analysis and aneuploidy level calculation

Expression (RNA-seq, CCLE\_expression), copy number variation (CCLE\_segment\_cn), and phenotype data was downloaded from the DepMap portal (https://depmap.org/portal/download/all/).

Since CCLE copy number was reported as the ratio between the copy number and the basal reference of the sample, a region with 2 copies of chromosomes will have a ratio of 1. The aneuploidy level was obtained by summing lreported ratio— $1\times$  segment length of the reported ratio within each sample. Expression was reported in the form of  $\log_2(TPM+1)$ .

#### Cell lines and tissue culture

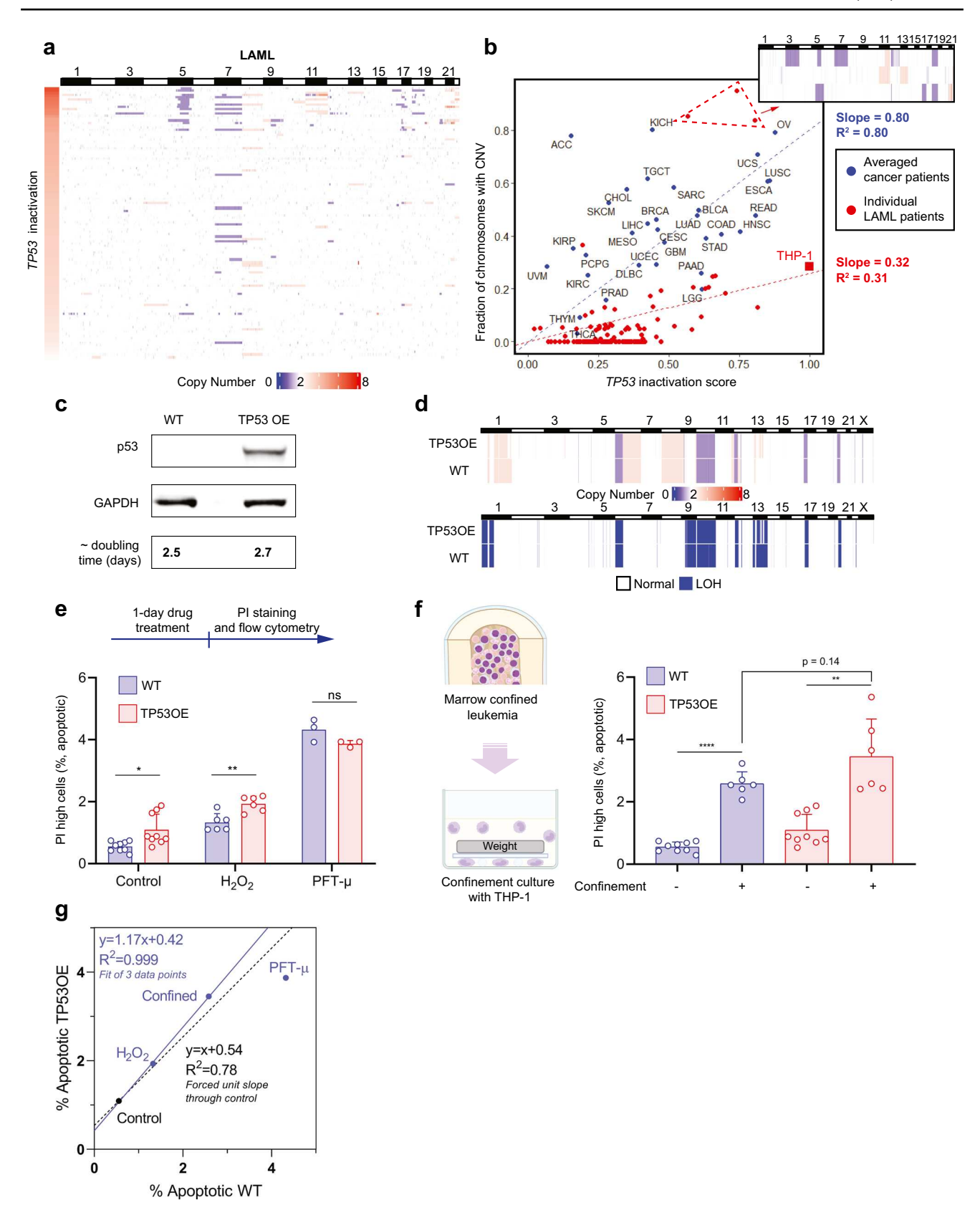
The following cell lines were used: THP-1 human leukemia monocytic cell line, B16-F10 murine melanoma cell line, U2OS human osteosarcoma cells, and A549 human lung adenocarcinoma cell line. All cell lines were obtained from American Type Culture Collection (THP-1: TIP-202; B16-F10: CRL-6322; U2OS: HTB-96; A549: CCL-185). THP-1 cells were cultured in RPMI 1640 (Gibco, Catalog no. 11879020); B16-F10 and U2OS in DMEM (Gibco, Catalog no. 10569010); and A549 in Ham's F-12 media (Gibco, Catalog no. 11765047). HEK293T cells used, acquired from ATCC, for lentiviral packaging were also cultured in DMEM. The media were supplemented with 10% (v/v) fetal bovine serum (FBS; MilliporeSigma, Catalog no. F2442) and 100 U mL<sup>-1</sup> penicillin–streptomycin (Gibco, Catalog no. 15140122). Both THP-1 and B16-F10 cells were passaged every 2-3 days. The density of THP-1 was maintained between 300,000 and 1.2 million cells/mL. B16-F10 cells were passaged using 0.05% Trypsin/EDTA (Gibco, Catalog no. 25300054). All cell lines were incubated at 37 °C and maintained at 5% CO<sub>2</sub>.

#### Single cell DNA-seq CNV analysis

DNA library was constructed using Chromium Single Cell DNA Reagent kits (PN-1000041, PN-1000057, PN-120262, PN-1000032, PN-1000036) from 10×Genomics (Pleasanton, CA) per the manufacturer's instructions. Library prepared was processed at the Next Generation Sequencing Core at the University of Pennsylvania (12–160, Translational Research Center, University of Pennsylvania) using NovaSeq 6000, 200 cycles (Illumina, San Diego, CA). For each sample, the copy number data was generated using Cell Ranger DNA pipeline (10×Genomics) and then exported to R to generate the copy number heatmap.

Cells were removed from the analysis if they were flagged as "noisy" by Cell Ranger. To ensure high confidence of the copy number profiles, cells with fewer than 600 k reads were excluded. Dimensional reduction was performed over integer single-cell copy number data using UMAP with R package "uwot" (v0.1.10, min\_dist=0, n\_neighbours=70). To identify the clones, we used the package "dbscan" (v1.1–10, minPts=3) to cluster. Heatmap was then generated using R package "ComplexHeatmap" (v2.11.1).







**◄Fig. 4** TP53 inactivation associates with cancer aneuploidy but trend is weaker for LAML patients. a TCGA-LAML patients' aneuploidy level scales with TP53 inactivation score. Each row represents the copy number profile of a single patients and was ordered from the highest to the lowest TP53 inactivation score. High score means more p53 inactivation. **b** TCGA analysis shows a linear correlation between aneuploidy level and TP53 inactivation with a R-squared value of 0.80. More TP53 inactivation leads to more CNV in different cancer types. Red data points represent individual LAML patients which demonstrate an intolerance toward CNV over LOH compared to the general trend. Red-dashed lines circled out outliers and their copy number profiles are shown in the inset. Table 1 reports the aneuploidy measure for each method used. c Western blot confirmed the success of TP53 transduction in THP-1. The transduced THP-1 has a slightly higher doubling time. d TP53-transduced THP-1 shows no significant difference in LOH and CNV profile compared to the wild-type THP-1. e TP53-transduced THP-1 has a higher cell death rate compared to the wild-type THP-1. The samples were then treated with hydrogen peroxide (H<sub>2</sub>O<sub>2</sub>) and pifithrin-µ (PFT-µ). The cell death percentage was measured using propidium iodide (PI) staining followed by flow cytometry. f Schematic representation of confining non-adherent THP-1 cell line to simulate marrow confined leukemia. Confinement leads to increased cell death in both wild-type and TP53-transduced THP-1. With TP53, though not significant, THP-1 has a tendency to have more cell death. g Percent of apoptotic cells of TP53-transduced THP-1 versus wild-type THP-1 in various treatment conditions. The dashed line indicates a strict proportionality with an offset set by the untreated cells (control)

#### Single cell RNA-seq

RNA libraries were prepared using the Chromium Single Cell Gene Expression kit (v3.1, single index, Catalog no. PN-1000128; PN-1000127; PN-1000213) from 10X Genomics (Pleasanton, CA) per the manufacturer's instructions. The libraries were sequenced at the Next Generation Sequencing Core (12-160, Translational Research Center, University of Pennsylvania) using NovaSeq 6000, 100 cycles (Illumina, San Diego, CA). Raw base call (BCL) files were analyzed using CellRanger (version 5.0.1) to generate FASTQ files and the "count" command was used to generate raw count matrices aligned to GRCh38. Cells were filtered to make sure that they expressed a minimum of 1400 genes with less than 15% mitochondrial content. Data was normalized using the "LogNormalize" method from the package "Seurat." Differential expression analysis was performed using the "FindAllMarkers" command and the output was used for gene set enrichment analysis (GSEA).

#### InferCNV analysis and reference dataset generation

Count matrix of single-cell RNA-seq results were used as input for inferCNV object construction (1.7.1) (InferCNV of the Trinity CTAT Project, https://github.com/broadinstitute/inferCNV). Gene position files were created for GRCh38. Single-cell RNA-seq data of healthy monocytes were used as reference for copy number profile construction.

The following dataset was used for reference generation: 10 k Peripheral Blood Mononuclear Cells (PBMCs) from a Healthy Donor, Single Indexed. The data was downloaded from the official website of 10×Genomics (Pleasanton, CA). Cells were filtered to make sure that they expressed a minimum of 1000 genes and a maximum of 6500 genes with less than 15% mitochondrial content. Cell types were annotated either manually or using the package "SingleR" (v1.6.1). For manual annotation, cells were clustered and assigned cell types based on the expression of cell type-specific signature genes (SI.5a). For SingleR, reference data was generated using the function "HumanPrimaryCellAtlasData" from the package "celldex" (v1.2.0) and compared to the raw expression matrix from the PBMCs to determine the cell types. A total of 1000 cells recognized as monocytes using both methods were selected as the reference for inferCNV analysis (SI. 5d-e). Aneuploidy types reported using various technologies and sources are in Table 1.

#### **Outlier detection**

Denoised results from inferCNV were used as the input ("infercnv.observations.txt"). The averaged copy number of each chromosome segment was calculated, and the difference between each cell's copy number and the overall mean at each segment was calculated. The deviation was summed across the entire chromosome and the distribution of the deviation was obtained. Cells sharing an absolute deviation that is more than 2.5 times standard deviation away from the distribution peak were marked to be outliers of a certain chromosome.

#### Single-nucleotide polymorphism arrays and analysis

Genomic DNA was isolated from 1 million cells with the Blood & Cell Culture DNA Mini Kit (Qiagen, Catalog no. 13323) per the manufacturer's instructions. The DNA samples were then sent to The Center for Applied Genomics Core (3615 Civic Ctr Blvd Abramson Pediatric Research Building, Suite 1016, Philadelphia, PA 19104) for single nucleotide polymorphism (SNP) array. For this array, > 650,000 probes have an average inter-probe distance of ~4 kb along the entire genome. For each sample, Genomics Core provided the data in the form of GenomeStudio files (Illumina). Chromosome copy number and LOH regions were reported in GenomeStudio (v2.0) using cnvPartition plug-in (v3.2.0, Illumina). The output was exported and analyzed using R. Heatmap was then generated using R package "ComplexHeatmap" (v2.11.1).

#### **Treatment**

For THP-1, the cells were suspended in non-treated plates (MedSupply Partners) at 300,000 cells/mL. The following



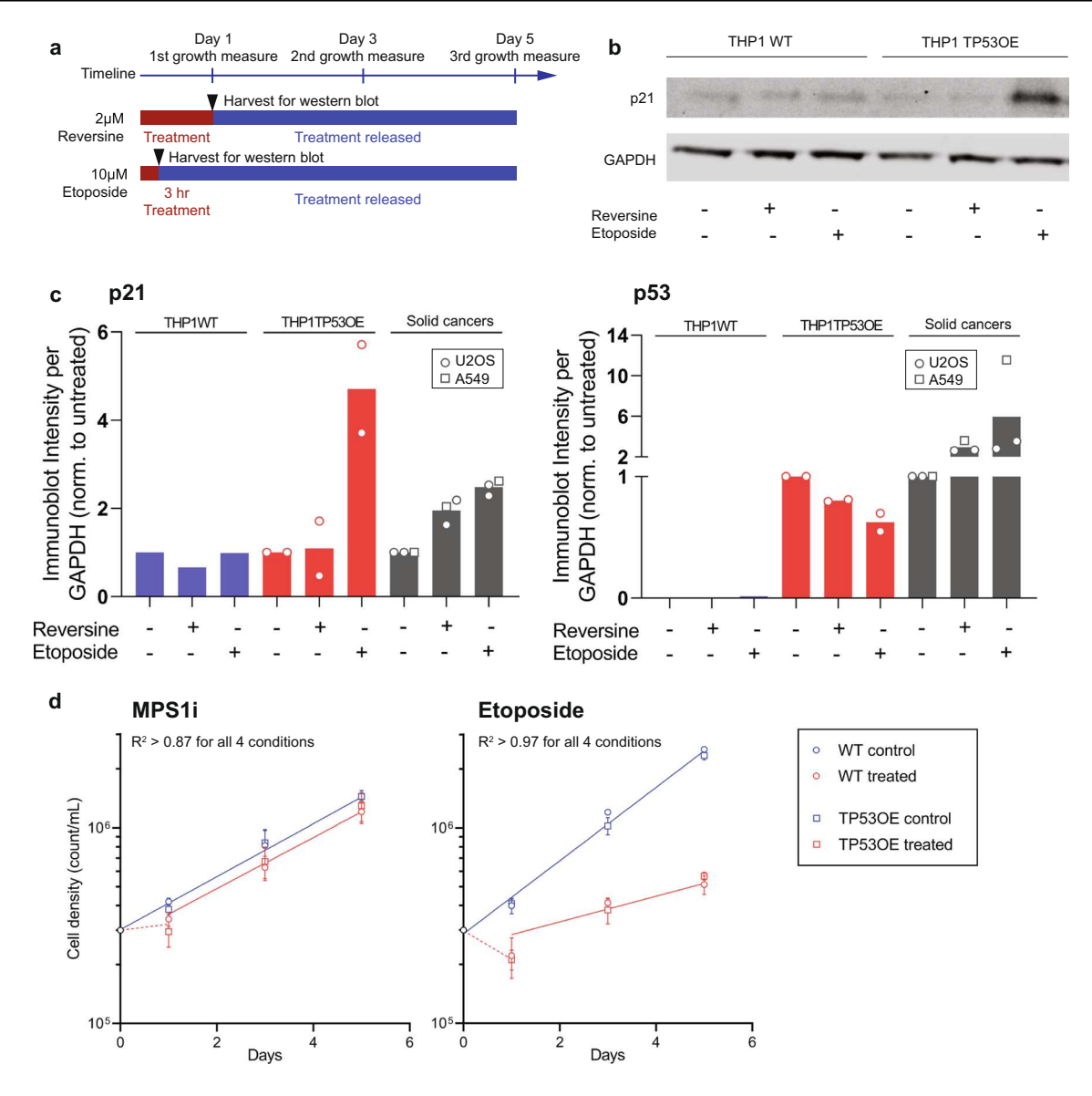


Fig. 5 p53 in engineered THP-1 responds to DNA damage in distinct patterns compared to the ones in adherent cancer cell lines. **a** Experimental setup of Western blot and cell proliferation measurements. THP-1 cells (wild-type and TP530E) were either treated with 2  $\mu$ M reversine for 1 day or treated with 10  $\mu$ M etoposide for 3 h. For Western blots, cell lysate was collected immediately after drug treatment. For cell proliferation measurements, 300,000 cells/mL at day 0 was followed by measurements at day 1, 3, and 5 (n=3). **b** Western blot shows p21 activation in TP53-transduced THP-1 under etoposide treatment. Wild-type THP-1 shows no significant p21 level changes.

c p21 and p53 Western blot intensity analysis. Each dot represents an independent Western blot experiment. Data from adherent cell lines (U2OS and A549) demonstrate a consistent trend of relative p21 and p53 levels when treated by reversine or etoposide. d Semi-log plot of growth of wild-type and *TP53*-transduced THP-1. Both wild-type and engineered THP-1 show the same response when being treated by reversine or etoposide. Reversine suppresses growth immediately after treatment but has little effect in later days. Etoposide kills cells and suppresses growth even after the drug release

chemical treatments were used: MPS1 inhibitor reversine (Cayman Chemical, Catalog no. 10004412),  $H_2O_2$  (Fisher Chemical, Catalog no. H323), Pifithrin- $\mu$  (PFT- $\mu$ , AmBeed, Catalog no. A370437), and dimethyl sulfoxide (DMSO; Millipore Sigma, Catalog no. D2438). The reversine concentrations and treatment times used are either 0.1  $\mu$ M continuous treatment or 2  $\mu$ M for 24 h followed by washout and 48 h

recovery.  $H_2O_2$  treatments were performed at 20  $\mu$ M for 24 h. PFT- $\mu$  treatment lasted 10  $\mu$ M for 24 h.

#### **Lentiviral packaging and delivery**

For p53 overexpression, the pLX313-TP53-WT plasmid was a gift from William Hahn and David Root (Addgene



plasmid # 118,014; http://n2t.net/addgene:118014; RRID: Addgene\_118014) (Giacomelli et al. 2018). Lentivirus was produced in HEK293T cells using MirusBio TransIT-Lenti Transfection Reagent (Catalog no. MIR 6604) following the manufacturer's protocol. Lentiviral production was allowed to occur for 48 h, after which the supernatant was collected. Infected cells were selected by incubation using 300  $\mu$ g/mL hygromycin (ThermoFisher, Catalog no. 10687010).

#### **Immunoblotting**

Standard Western blotting was performed. In brief, THP-1 cells were centrifuged and washed 2× with cold PBS, and then lysed in RIPA buffer (Sigma, Catalog no. R0278) containing 1 x protease inhibitor cocktail (Sigma, Catalog no. P8340), followed by 30-min centrifugation. Supernatant was boiled in 1×NuPage LDS sample buffer (Invitrogen, Catalog no. NP0007) with 2.5% v/v  $\beta$ -mercaptoethanol. Approximately 1 million cells were used for each analysis. Proteins were separated by electrophoresis in NuPAGE 4-12% Bis-Tris gels run with 1×MOPS buffer (Invitrogen, Catalog no. NP0323) and transferred to an iBlot nitrocellulose membrane (Invitrogen, Catalog no. IB301002). The membranes were then blocked with 5% non-fat milk in Tris-buffered saline (TBS) plus Tween-20 (TBST) for 1 h. The membranes were washed with TBST and incubated with 1:1000 primary antibody in 5% milk in TBST overnight at 4 °C. The membranes were then incubated with 1:10,000 IRDye 800CW (LI-COR Bioscience) in 5% milk in TBST for 1 h at room temperature with agitation. Developed membranes were scanned using Odyssey M system (LI-COR Bioscience) and analyzed with ImageJ (National Institutes of Health).

#### Immunofluorescence and imaging

For A549, cells were fixed for 15 min in 4% formaldehyde (Thermo Fisher Scientific, Catalog no. 28908), permeabilized by 0.5% Triton-X (MilliporeSigma, Catalog no. 112298) for 15 min, and blocked for 30 min with 5% bovine serum albumin (BSA, MilliporeSigma, Catalog no. A7906). The sample was then incubated overnight in primary antibodies (1:500 dilution). For p53 staining, the primary antibody used was DO-1 (Santa Cruz, Catalog no. sc-126). The cells were then incubated in secondary antibodies (1:500 dilution) for 1.5 h, and their nuclei were stained with 8 µM Hoechst 33,342 (Thermo Fisher, Catalog no. 62249) for 15 min. For THP-1, the cells were centrifuged, fixed with 4% formaldehyde for 20 min, and washed twice with deionized water. Three drops of cell suspension solution were then dispensed on gelatin-coated microscope slides and dried on a hot plate. Hydrophobic barrier pen was used to surround the cell spot, and the rest of the procedures were the same as

A549 staining. Epifluorescence imaging was performed using an Olympus IX71 with a digital camera (Photometrics) and a  $20 \times /0.6$  NA object.

#### **Confinement assay**

Thirty-millimeter glass coverslips were coated with RainX (glass water repellent PDMS; RainX Company, Catalog no. 1597562), left in PBS, and sterilized overnight with ultraviolet light. The following day, THP-1 cells were resuspended at 2,000,000 cells/mL. Six to 7  $\mu$ m polystyrene beads (SpheroTech, Catalog no. SVP-60–5) were added at a density of 7  $\mu$ L of beads/2 mL of media to act as spacers to control the height of the confinement. A 300  $\mu$ L droplet of the cell and bead suspension was pipetted in an untreated 6-well plate, and the coverslip was placed on top of the droplet. A sterilized stainless-steel weight was placed on top of the coverslip, and 1 mL of media was added to the well. After 8 h, the confinement setup was removed.

#### Flow cytometry and analysis

All flow cytometry was performed on a BD LSRII (Benton Dickinson) located at Penn Cytomics and Cell Sorting Resource Laboratory (297 John Morgan Building, Philadelphia, PA 19104). Exported FACS files were analyzed using FCS Express  $7^{th}$  edition. For a cell death assay, THP-1 cells were centrifuged and resuspended in FACS buffer (PBS+5% FBS) with 1  $\mu$ g/mL Propdium Iodide (PI, Sigma, Catalog no. P4864), and analyzed by flow cytometry.

To remove aggregates from the analysis, forward scatter parameters FSC-A vs FSC-H and side scatter parameters SSC-A vs SSC-H were used in gating. Intact cells were filtered out by gating on forward scatter and side scatter (FSC-A vs SSC-A). Cell death percentage were obtained by quantifying the cell that is high in PI staining.

#### Statistics and reproducibility

The statistical methods for each experiment are included in the corresponding figure legends. All statistical analyses were done on GraphPad Prism 9.0. Unless specified, all error bars in the plots are standard deviation. All experiments were biologically repeated and confirmed.

**Supplementary Information** The online version contains supplementary material available at https://doi.org/10.1007/s00412-023-00800-y.

Acknowledgements The authors acknowledge the following University of Pennsylvania core facilities: Cell Center Stockroom, the Penn Cytomics and Cell Sorting Resource Laboratory, and the Penn Genomic Analysis Core. We also acknowledge The Center for Applied Genomics Core in The Children's Hospital of Philadelphia for SNPa's.



Author contribution Mai Wang performed experimental work, data analysis, figure construction, and contributed to conceptualization and design of the study. Steven Phan performed experimental work, analyzed data, and contributed to the figure construction. Brandon H. Hayes performed experimental work. Dennis E. Discher designed, conceptualized, and supervised the study. The manuscript was written by Mai Wang and Dennis E. Discher. All authors read and approved the final manuscript.

Funding This work was supported by funding from the National Institutes of Health/National Cancer Institute (U54 CA193417, U01 CA254886, P01 CA265794), NHLBI (R01 HL124106), NSF GRFP DGE-1845298 (BHH), National Science Foundation (MRSEC DMR-1720530 and DMR-1420530 and Grant Agreements CMMI 1548571 and 154857), Human Frontier Science Program Grant RGP00247/2017, and Pennsylvania Department of Health Grant HRFF 4100083101.

**Data Availability** All data generated or analyzed during this study are included in this published article. All materials generated are available from the corresponding author on reasonable request.

#### **Declarations**

Competing interests The authors declare no competing interests.

Ethical approval Not applicable.

Consent to participate Not applicable.

Consent for publication Not applicable.

**Conflict of interest** The authors declare no competing interests.

#### References

- Aubrey BJ, Kelly GL, Janic A, Herold MJ, Strasser A (2018) How does p53 induce apoptosis and how does this relate to p53-mediated tumour suppression? Cell Death Differ 25(1):104–113. https://doi.org/10.1038/cdd.2017.169
- Avery-Kiejda KA, Morten B, Wong-Brown MW, Mathe A, Scott RJ (2014) The relative mRNA expression of p53 isoforms in breast cancer is associated with clinical features and outcome. Carcinogenesis 35(3):586–596. https://doi.org/10.1093/carcin/bgt411
- Baslan T, Morris JPt, Zhao Z, Reyes J, Ho YJ, Tsanov KM, Bermeo J, Tian S, Zhang S, Askan G, Yavas A, Lecomte N, Erakky A, Varghese AM, Zhang A, Kendall J, Ghiban E, Chorbadjiev L, Wu J, ... Lowe SW (2022) Ordered and deterministic cancer genome evolution after p53 loss. Nature 608(7924):795-802. https://doi.org/10.1038/s41586-022-05082-5
- Bejarano I, Espino J, Marchena AM, Barriga C, Paredes SD, Rodriguez AB, Pariente JA (2011) Melatonin enhances hydrogen peroxide-induced apoptosis in human promyelocytic leukaemia HL-60 cells. Mol Cell Biochem 353(1–2):167–176. https://doi.org/10.1007/s11010-011-0783-8
- Ben-David U, Amon A (2020) Context is everything: aneuploidy in cancer. Nat Rev Genet 21(1):44–62. https://doi.org/10.1038/s41576-019-0171-x
- Beroukhim R, Mermel CH, Porter D, Wei G, Raychaudhuri S, Donovan J, Barretina J, Boehm JS, Dobson J, Urashima M, Mc Henry KT, Pinchback RM, Ligon AH, Cho YJ, Haery L, Greulich H, Reich M, Winckler W, Lawrence MS, ... Meyerson M (2010) The

- landscape of somatic copy-number alteration across human cancers. Nature 463(7283):899–905. https://doi.org/10.1038/nature08822
- Bolton H, Graham SJL, Van der Aa N, Kumar P, Theunis K, Fernandez Gallardo E, Voet T, Zernicka-Goetz M (2016) Mouse model of chromosome mosaicism reveals lineage-specific depletion of aneuploid cells and normal developmental potential. Nat Commun 7:11165. https://doi.org/10.1038/ncomms11165
- Bourdon JC, Khoury MP, Diot A, Baker L, Fernandes K, Aoubala M, Quinlan P, Purdie CA, Jordan LB, Prats AC, Lane DP, Thompson AM (2011) p53 mutant breast cancer patients expressing p53gamma have as good a prognosis as wild-type p53 breast cancer patients. Breast Cancer Res 13(1):R7. https://doi.org/10.1186/bcr2811
- Buscemi G, Ricci C, Zannini L, Fontanella E, Plevani P, Delia D (2014) Bimodal regulation of p21(waf1) protein as function of DNA damage levels. Cell Cycle 13(18):2901–2912. https://doi.org/10.4161/15384101.2014.946852
- Chipuk JE, Kuwana T, Bouchier-Hayes L, Droin NM, Newmeyer DD, Schuler M, Green DR (2004) Direct activation of Bax by p53 mediates mitochondrial membrane permeabilization and apoptosis. Science 303(5660):1010–1014. https://doi.org/10.1126/science.1092734
- Cimini D, Howell B, Maddox P, Khodjakov A, Degrassi F, Salmon ED (2001) Merotelic kinetochore orientation is a major mechanism of aneuploidy in mitotic mammalian tissue cells. J Cell Biol 153(3):517–527. https://doi.org/10.1083/jcb.153.3.517
- Davoli T, Xu AW, Mengwasser KE, Sack LM, Yoon JC, Park PJ, Elledge SJ (2013) Cumulative haploinsufficiency and triplosensitivity drive aneuploidy patterns and shape the cancer genome. Cell 155(4):948–962. https://doi.org/10.1016/j.cell.2013.10.011
- Dudka D, Noatynska A, Smith CA, Liaudet N, McAinsh AD, Meraldi P (2018) Complete microtubule-kinetochore occupancy favours the segregation of merotelic attachments. Nat Commun 9(1):2042. https://doi.org/10.1038/s41467-018-04427-x
- Duijf PH, Schultz N, Benezra R (2013) Cancer cells preferentially lose small chromosomes. Int J Cancer 132(10):2316–2326. https://doi.org/10.1002/ijc.27924
- Emon B, Bauer J, Jain Y, Jung B, Saif T (2018) Biophysics of tumor microenvironment and cancer metastasis a mini review. Comput Struct Biotechnol J 16:279–287. https://doi.org/10.1016/j.csbj.2018.07.003
- Engeland K (2022) Cell cycle regulation: p53-p21-RB signaling. Cell Death Differ 29(5):946-960. https://doi.org/10.1038/s41418-022-00988-z
- Fu X, Wu S, Li B, Xu Y, Liu J (2020) Functions of p53 in pluripotent stem cells. Protein Cell 11(1):71–78. https://doi.org/10.1007/s13238-019-00665-x
- Giacomelli AO, Yang X, Lintner RE, McFarland JM, Duby M, Kim J, Howard TP, Takeda DY, Ly SH, Kim E, Gannon HS, Hurhula B, Sharpe T, Goodale A, Fritchman B, Steelman S, Vazquez F, Tsherniak A, Aguirre AJ, ... Hahn WC (2018) Mutational processes shape the landscape of TP53 mutations in human cancer. Nat Genet 50(10):1381–1387. https://doi.org/10.1038/s41588-018-0204-y
- Goldman MJ, Craft B, Hastie M, Repecka K, McDade F, Kamath A, Banerjee A, Luo Y, Rogers D, Brooks AN, Zhu J, Haussler D (2020) Visualizing and interpreting cancer genomics data via the Xena platform. Nat Biotechnol 38(6):675–678. https://doi. org/10.1038/s41587-020-0546-8
- Gonzales F, Cheok MH (2018) Impact of CNA on AML prognosis. Oncotarget 9(16):12540–12541. https://doi.org/10.18632/oncotarget.23404
- Hinchcliffe EH, Day CA, Karanjeet KB, Fadness S, Langfald A, Vaughan KT, Dong Z (2016) Chromosome missegregation during anaphase triggers p53 cell cycle arrest through histone H3.3



Ser31 phosphorylation. Nat Cell Biol 18(6):668–675. https://doi.org/10.1038/ncb3348

- Ivanovska IL, Swift J, Spinler K, Dingal D, Cho S, Discher DE (2017) Cross-linked matrix rigidity and soluble retinoids synergize in nuclear lamina regulation of stem cell differentiation. Mol Biol Cell 28(14):2010–2022. https://doi.org/10.1091/mbc.E17-01-0010
- Joruiz SM, Bourdon JC (2016) p53 isoforms: key regulators of the cell fate decision. Cold Spring Harb Perspect Med 6(8). https:// doi.org/10.1101/cshperspect.a026039
- Kaiser M, Kuhnl A, Reins J, Fischer S, Ortiz-Tanchez J, Schlee C, Mochmann LH, Heesch S, Benlasfer O, Hofmann WK, Thiel E, Baldus CD (2011) Antileukemic activity of the HSP70 inhibitor pifithrin-mu in acute leukemia. Blood Cancer J 1(7):e28. https:// doi.org/10.1038/bcj.2011.28
- Knijnenburg TA, Wang L, Zimmermann MT, Chambwe N, Gao GF, Cherniack AD, Fan H, Shen H, Way GP, Greene CS, Liu Y, Akbani R, Feng B, Donehower LA, Miller C, Shen Y, Karimi M, Chen H, Kim P, ... Wang C (2018) Genomic and molecular landscape of DNA damage repair deficiency across The Cancer Genome Atlas. Cell Rep 23(1):239–254 e236. https://doi.org/10.1016/j.celrep.2018.03.076
- Lane DP, Cheok CF, Lain S (2010) p53-based cancer therapy. Cold Spring Harb Perspect Biol 2(9):a001222. https://doi.org/10.1101/cshperspect.a001222
- Lee SJ, Ahn H, Nam KW, Kim KH, Mar W (2012) Effects of rutaecarpine on hydrogen peroxide-induced apoptosis in murine hepa-1c1c7 cells. Biomol Ther (seoul) 20(5):487–491. https:// doi.org/10.4062/biomolther.2012.20.5.487
- Leu JI, Dumont P, Hafey M, Murphy ME, George DL (2004) Mitochondrial p53 activates Bak and causes disruption of a Bak-Mc11 complex. Nat Cell Biol 6(5):443–450. https://doi.org/10.1038/ncb1123
- Li F, Wang J, Liu A, Xin L, Zhong S, Hong Y, Chen Y (2019) Prolonged lumbosacral pain as the initial presentation in acute lymphoblastic leukemia in an adult: a case report. Medicine (Baltimore) 98(24):e15912. https://doi.org/10.1097/MD.0000000000015912
- Li Z, Zhao J, Li Q, Yang W, Song Q, Li W, Liu J (2010) KLF4 promotes hydrogen-peroxide-induced apoptosis of chronic myeloid leukemia cells involving the bcl-2/bax pathway. Cell Stress Chaperones 15(6):905–912. https://doi.org/10.1007/s12192-010-0199-5
- Liu X, Winey M (2012) The MPS1 family of protein kinases. Annu Rev Biochem 81:561–585. https://doi.org/10.1146/annurev-bioch em-061611-090435
- Lukow DA, Sausville EL, Suri P, Chunduri NK, Wieland A, Leu J, Smith JC, Girish V, Kumar AA, Kendall J, Wang Z, Storchova Z, Sheltzer JM (2021) Chromosomal instability accelerates the evolution of resistance to anti-cancer therapies. Dev Cell 56(17):2427-2439 e2424. https://doi.org/10.1016/j.devcel.2021.07.009
- Lundberg A, Yi JJJ, Lindstrom LS, Tobin NP (2022) Reclassifying tumour cell cycle activity in terms of its tissue of origin. NPJ Precis Oncol 6(1):59. https://doi.org/10.1038/s41698-022-00302-7
- Mierke CT, Sauer F, Grosser S, Puder S, Fischer T, Kas JA (2018) The two faces of enhanced stroma: stroma acts as a tumor promoter and a steric obstacle. NMR Biomed 31(10):e3831. https://doi.org/10.1002/nbm.3831
- Mihara M, Erster S, Zaika A, Petrenko O, Chittenden T, Pancoska P, Moll UM (2003) p53 has a direct apoptogenic role at the mitochondria. Mol Cell 11(3):577–590. https://doi.org/10.1016/s1097-2765(03)00050-9
- Ponnapalli SP, Bradley MW, Devine K, Bowen J, Coppens SE, Leraas KM, Milash BA, Li F, Luo H, Qiu S, Wu K, Yang H, Wittwer CT, Palmer CA, Jensen RL, Gastier-Foster JM, Hanson HA, Barnholtz-Sloan JS, Alter O (2020) Retrospective clinical trial experimentally validates glioblastoma genome-wide pattern of DNA copy-number alterations predictor of survival. APL Bioeng 4(2):026106. https://doi.org/10.1063/1.5142559
- Prokocimer M, Molchadsky A, Rotter V (2017) Dysfunctional diversity of p53 proteins in adult acute myeloid leukemia: projections on

- diagnostic workup and therapy. Blood 130(6):699–712. https://doi.org/10.1182/blood-2017-02-763086
- Roy P, Reavey E, Rayne M, Roy S, Abed El Baky M, Ishii Y, Bartholomew C (2010) Enhanced sensitivity to hydrogen peroxide-induced apoptosis in Evi1 transformed Rat1 fibroblasts due to repression of carbonic anhydrase III. FEBS J 277(2):441–452. https://doi.org/10.1111/j.1742-4658.2009.07496.x
- Santaguida S, Richardson A, Iyer DR, M'Saad O, Zasadil L, Knouse KA, Wong YL, Rhind N, Desai A, Amon A (2017) Chromosome mis-segregation generates cell-cycle-arrested cells with complex karyotypes that are eliminated by the immune system. Dev Cell 41(6):638-651 e635. https://doi.org/10.1016/j.devcel.2017.05.022
- Shah SB, Carlson CR, Lai K, Zhong Z, Marsico G, Lee KM, Félix Vélez NE, Abeles EB, Allam M, Hu T, Walter LD, Martin KE, Gandhi K, Butler SD, Puri R, McCleary-Wheeler AL, Tam W, Elemento O, Takata K, Steidl C, Scott DW, Fontan L, Ueno H, Cosgrove BD, Inghirami G, García AJ, Coskun AF, Koff JL, Melnick A, Singh A (2023) Combinatorial treatment rescues tumourmicroenvironment-mediated attenuation of MALT1 inhibitors in B-cell lymphomas. Nat Mater 22:511–523. https://doi.org/10.1038/s41563-023-01495-3
- Shi T, van Soest DMK, Polderman PE, Burgering BMT, Dansen TB (2021) DNA damage and oxidant stress activate p53 through differential upstream signaling pathways. Free Radic Biol Med 172:298–311. https://doi.org/10.1016/j.freeradbiomed.2021.06. 013
- Sies H, Jones DP (2020) Reactive oxygen species (ROS) as pleiotropic physiological signalling agents. Nat Rev Mol Cell Biol 21(7):363–383. https://doi.org/10.1038/s41580-020-0230-3
- Steele CD, Abbasi A, Islam SMA, Bowes AL, Khandekar A, Haase K, Hames-Fathi S, Ajayi D, Verfaillie A, Dhami P, McLatchie A, Lechner M, Light N, Shlien A, Malkin D, Feber A, Proszek P, Lesluyes T, Mertens F, ... Pillay N (2022) Signatures of copy number alterations in human cancer. Nature 606(7916):984–991. https://doi.org/10.1038/s41586-022-04738-6
- Stucke VM, Sillje HH, Arnaud L, Nigg EA (2002) Human Mps1 kinase is required for the spindle assembly checkpoint but not for centrosome duplication. EMBO J 21(7):1723–1732. https://doi.org/10.1093/emboj/21.7.1723
- Sugimoto K, Toyoshima H, Sakai R, Miyagawa K, Hagiwara K, Ishi-kawa F, Takaku F, Yazaki Y, Hirai H (1992) Frequent mutations in the p53 gene in human myeloid leukemia cell lines. Blood 79(9):2378–2383. https://www.ncbi.nlm.nih.gov/pubmed/1571549
- Toufektchan E, Toledo F (2018) The guardian of the genome revisited: p53 downregulates genes required for telomere maintenance, DNA repair, and centromere structure. Cancers (Basel) 10(5). https://doi.org/10.3390/cancers10050135
- van Dijk E, van den Bosch T, Lenos KJ, El Makrini K, Nijman LE, van Essen HFB, Lansu N, Boekhout M, Hageman JH, Fitzgerald RC, Punt CJA, Tuynman JB, Snippert HJG, Kops G, Medema JP, Ylstra B, Vermeulen L, Miedema DM (2021) Chromosomal copy number heterogeneity predicts survival rates across cancers. Nat Commun 12(1):3188. https://doi.org/10.1038/s41467-021-23384-6
- Wagenblast E, Araujo J, Gan OI, Cutting SK, Murison A, Krivdova G, Azkanaz M, McLeod JL, Smith SA, Gratton BA, Marhon SA, Gabra M, Medeiros JJF, Manteghi S, Chen J, Chan-Seng-Yue M, Garcia-Prat L, Salmena L, De Carvalho DD, ... Lechman ER (2021) Mapping the cellular origin and early evolution of leukemia in Down syndrome. Science, 373(6551). https://doi.org/10.1126/science.abf6202
- Walles SA, Zhou R, Liliemark E (1996) DNA damage induced by etoposide; a comparison of two different methods for determination of strand breaks in DNA. Cancer Lett 105(2):153–159. https://doi.org/10.1016/0304-3835(96)04266-8



Wallis B, Bowman KR, Lu P, Lim CS (2023) The challenges and prospects of p53-based therapies in ovarian cancer. Biomolecules 13(1). https:// doi.org/10.3390/biom13010159

- Weaver BA, Silk AD, Montagna C, Verdier-Pinard P, Cleveland DW (2007) Aneuploidy acts both oncogenically and as a tumor suppressor. Cancer Cell 11(1):25–36. https://doi.org/10.1016/j.ccr. 2006.12.003
- Wei B, Zhou X, Liang C, Zheng X, Lei P, Fang J, Han X, Wang L, Qi C, Wei H (2017) Human colorectal cancer progression correlates with LOX-induced ECM stiffening. Int J Biol Sci 13(11):1450–1457. https://doi.org/10.7150/ijbs.21230
- Welch JS (2018) Patterns of mutations in TP53 mutated AML. Best Pract Res Clin Haematol 31(4):379–383. https://doi.org/10.1016/j.beha.2018.09.010
- Wong SW, Lenzini S, Shin JW (2018) Perspective: biophysical regulation of cancerous and normal blood cell lineages in hematopoietic malignancies. APL Bioeng 2(3):031802. https://doi.org/10.1063/1.5025689
- Xia Y, Ivanovska IL, Zhu K, Smith L, Irianto J, Pfeifer CR, Alvey CM, Ji J, Liu D, Cho S, Bennett RR, Liu AJ, Greenberg RA, Discher

- DE (2018) Nuclear rupture at sites of high curvature compromises retention of DNA repair factors. J Cell Biol 217(11):3796–3808. https://doi.org/10.1083/jcb.201711161
- Xian S, Dosset M, Almanza G, Searles S, Sahani P, Waller TC, Jepsen K, Carter H, Zanetti M (2021) The unfolded protein response links tumor aneuploidy to local immune dysregulation. EMBO Rep 22(12):e52509. https://doi.org/10.15252/embr.202152509
- Zhou L, Jilderda LJ, Foijer F (2020) Exploiting aneuploidy-imposed stresses and coping mechanisms to battle cancer. Open Biol 10(9):200148. https://doi.org/10.1098/rsob.200148

**Publisher's note** Springer Nature remains neutral with regard to jurisdictional claims in published maps and institutional affiliations.

Springer Nature or its licensor (e.g. a society or other partner) holds exclusive rights to this article under a publishing agreement with the author(s) or other rightsholder(s); author self-archiving of the accepted manuscript version of this article is solely governed by the terms of such publishing agreement and applicable law.

